Astronomy Letters, Vol. 26, No. 2, 2000, pp. 77–87. Translated from Pis'ma v Astronomicheskiĭ Zhurnal, Vol. 26, No. 2, 2000, pp. 102–114.

The Supernova Remnant G78.2+2.1: New Optical and X-ray Observations

T. A. Lozinskaya[1], V. V. Pravdikova[1], and A. V. Finoguenov[2]

[1] *Sternberg Astronomical Institute, Universitetskiĭ pr. 13, Moscow, 119899 Russia*
[2] *Space Research Institute, Russian Academy of Sciences, ul. Profsoyuznaya 84/32, Moscow, 117810 Russia*

Received May 11, 1999; in final form, June 9, 1999

Abstract—New optical and X-ray observations of the supernova remnant (SNR) G78.2+2.1 are presented. CCD Hα observations with a Fabry–Perot interferometer attached to the 125-cm reflector at the Crimean Station of the Sternberg Astronomical Institute are used to obtain the radial-velocity field toward the SNR and in its vicinity. The brightness distribution and X-ray spectrum of the SNR are obtained from archival ROSAT and ASCA X-ray data. The X-ray image of G78.2+2.1 exhibits a shell structure ($\Delta R/R \simeq 0.3$) and is generally similar to its radio image; a comparison with the radio map at $\nu = 1.4$ GHz constructed from archival VLA data reveals the coincidence of features on scales of several arcminutes at the eastern boundary of G78.2+2.1. Weak X-ray emission (an outer shell or a halo of size $\simeq 2°$) has been identified for the first time far outside G78.2+2.1. The X-ray emission from G78.2+2.1 is shown to characterize a young adiabatic SNR [$M_{X-ray} \simeq 100 M_\odot$, $V_s \simeq 10^3$ km s^{-1}, $t \simeq (5–6) \times 10^3$ years], which probably expands inside the cavity swept up by the progenitor's stellar wind. Searches for the corresponding radio structure are required to elucidate the nature of the outer X-ray shell or halo. © *2000 MAIK "Nauka/Interperiodica".*

1. INTRODUCTION

The supernova remnant (SNR) G78.2+2.1 (see [1–4] and references therein) lies in the sky area toward the Cyg X complex that is most difficult to study. Since this area has a complex structure, where more than forty H II regions and a large number of shell structures of various scales are concentrated, the SNR G78.2+2.1 was not identified immediately; there is still a confusion of names in present-day literature. The brightest radio source DR4 in the complex and the associated 3′ nebula near γ Cygni [5] were originally believed to be the SNR.

However, the spectroscopic and interferometric observations of the nebula near γ Cygni by Lozinskaya [6] and Johnson [7] showed this to be an H II region rather than a SNR; the ionizing star was also found at its center [8, 9]. To explain the nonthermal radio emission from an "ordinary" H II region, Lozinskaya [10] suggested that it was overrun by an expanding shell, the remnant of a supernova exploded nearby. Higgs *et al.* [1] and Baars *et al.* [11] actually found a ~1° radio shell of G78.2+2.1 with a synchrotron spectrum. The source DR4 constitutes the brightest southeastern part of G78.2+2.1, and its radio emission consists of two components, thermal and nonthermal.

Here, we present our Hα Fabry–Perot observations of the region and reduce the archival ROSAT and ASCA X-ray data for G78.2+2.1. We also use the archival VLA data for the eastern part of G78.2+2.1.

Section 2 describes the technique of interferometric observations and presents the results of our study of the radial-velocity field toward the SNR and in its vicinity. The X-ray observations of G78.2+2.1 are reduced in Sect. 3. The data and the conclusions concerning the SNR nature that follow from them are discussed in Sect. 4.

2. INTERFEROMETRIC Hα OBSERVATIONS

2.1. Observing and Reduction Techniques

We studied the radial-velocity field in Hα by using a Fabry–Perot interferometer with a CCD at the Cassegrain focus of the 125-cm reflector at the Crimean Station of the Sternberg Astronomical Institute. The pre-monochromatization was carried out by means of an interference filter with a FWHM of ≃20 Å. The field of view and the angular resolution were, respectively, 10′ and 3–4″; the actual spectral resolution corresponded to ≃15 km s^{-1}. The free dispersion region (the radial-velocity range free from the overlapping of adjacent interference orders) was ~800 km s^{-1}; the [N II] 6584 Å line was in the middle of this range and was clearly separated from Hα, whose largest zero-level width did not exceed 200 km s^{-1} everywhere in the region under study.

The line profile was fitted with one or more Gaussians by assuming that the FWHM of each component was larger than the FWHM of the instrumental profile and that the signal-to-noise ratio was ≥5. In 1997–1998, we obtained 23 interferograms in a large area including the SNR G78.2+21. We also used the observations of

1063-7737/00/2602-0077$20.00 © 2000 MAIK "Nauka/Interperiodica"

the bright nebula near γ Cygni performed by Lozinskaya [6] with the same Fabry–Perot interferometer at the focus of the 125-cm reflector; the only difference was the use of an image intensifier instead of a CCD array as the light detector. In 1974, a total of eight Hα interferograms and five [N II] interferograms were taken; the total number of previous velocity measurements exceeds 100.

The localization of the interferometric rings of the Hα and [N II] lines in the G78.2+2.1 image is shown in Fig. 1. Also shown in this figure is the localization of rings for the nearby Cygnus X region, which mainly falls within the X-ray shell we identified (see Subsect. 3.2). For a comparison with velocities in the extended Cygnus X region, we used about 40 more Hα images outside the boundaries of Fig. 1.

2.2. Results of the Hα Observations

The H II velocity measurements based on the 1997–1998 observations are shown in Fig. 2 in the form of radial-velocity histograms for the Hα components. Figures 2a and 2b correspond, respectively, to the SNR G78.2+2.1 and to the nearby regions of the Cygnus X complex outside the bright SNR but inside the weak outer X-ray shell identified in Subsect. 3.2.

We see from Fig. 2a that the characteristic H II radial velocity toward G78.2+2.1 lies in the range $V(\mathrm{LSR}) = 0$–10 km s^{-1} at half maximum of the histogram. At the same time, a group of negative radial velocities, $V(\mathrm{LSR}) = -(45$–$20)$ km s^{-1}, is clearly identified. The mean velocities corresponding to the two peaks in the histogram are $V_1 = 2.6 \pm 4.3$ km s^{-1} (for 109 measurements) and $V_2 = -34.7 \pm 7.9$ (for 21 measurements).

A comparison of the velocity distributions for the bright SNR (Fig. 2a) and for the weak outer X-ray shell (Fig. 2b) reveals no statistically significant differences. Velocities from $V(\mathrm{LSR}) = -5$ to $V(\mathrm{LSR}) = +15$ km s^{-1} at half maximum of the histogram are observed in the outer region; the mean velocity is $V(\mathrm{LSR}) = 6.0 \pm 4.2$ km s^{-1}. A component at $V(\mathrm{LSR}) = -(50$–$20)$ km s^{-1} with a mean velocity of -34 km s^{-1} is also distinguished in the histogram of Fig. 2b.

The Hα and [N II] profiles for the bright nebula near γ Cygni turned out to be single. The mean velocity of the nebula is $V(\mathrm{LSR}) = 9 \pm 3$ km s^{-1}; the mean velocity of the nearby bright H II regions of the radio source DR4 (at distances no larger than 10′ from the nebular boundary) is $V(\mathrm{LSR}) = -2 \pm 2$ km s^{-1}. These measurements agree, within the error limits, with $V(\mathrm{LSR}) \simeq 5$ km s^{-1} obtained by Johnson [7] from a single interferogram of the γ Cygni nebula. The velocities near the radio source DR4 and the γ Cygni nebula are seen to match those of the main component in the diagram of Fig. 2a for the extended SNR G78.2+2.1.

When making a comparison with the velocity field in the Cygnus X complex outside G78.2+2.1 and the weak outer shell, we made sure that a single line was manly observed in the east and in the west in the velocity range from 2.5 to 17. 5 km s^{-1} with a mean velocity of 10 ± 4.2 km s^{-1}. The corresponding histogram for distances between 2° and 4° from the SNR center is shown in Fig. 2c. At the same time, local regions with high-velocity gas motions are encountered east and north of G78.2+2.1, i.e., closer to the Cygnus X center. They are probably associated with additional sources of mechanical energy or with large-scale motions of a different origin; their discussion is beyond the scope of our study. We therefore collected the velocities of these "peculiar" regions in the histogram of Fig. 2d solely to emphasize that high velocities in the range from -35 to $+35$ km s^{-1} are observed not only toward the SNR. Similar mean velocities were obtained for Cygnus X from radio recombination-line observations: The group of sources DR 18, 20, 21, 22, and 23 has the mean velocity $V_{166\alpha} = 6$ km s^{-1}; and the group of IC 1318b, c, DR 6, 9, 12, 13, and 15 has the mean velocity $V_{166\alpha} = -5$ km s^{-1} [12]. The mean velocity of the Cygnus X complex as inferred from the $H_{110\alpha}$ measurements by Piepenbrink and Wendker [13] is -2.9 km s^{-1} (see also [14]).

Thus, our Hα measurements have shown that there is agreement between the velocities toward the G78.2+2.1 shell, for its bright southeastern part near γ Cygni, and for the outer weak X-ray shell.

Our measured high H II velocities toward the SNR are confirmed by 21-cm observations: Landecker *et al.* [15] and Braun and Strom [16] detected high-velocity H I clouds of small angular sizes here. The high velocity of the shock triggered by the SNR expansion is also suggested by the X-ray observations presented in Sect. 3. Nevertheless, since high H II velocities are observed not only toward the SNR but also outside it in the central region of Cygnus X, we cannot unequivocally relate the detected high velocities to G78.2+2.1.

3. X-RAY EMISSION FROM THE SUPERNOVA REMNANT

X-ray emission from the bright southeastern part of G78.2+2.1 was observed from the Einstein Observatory [17]. The ROSAT images of G78.2+2.1 were published in [18, 19] but without quantitative estimates, only to localize the gamma-ray source 2EG J2020+4026 and the associated compact X-ray source.

3.1. The Archival ROSAT and ASCA Data and Their Reduction

We analyzed the archival data for G78.2+2.1 from two X-ray observatories: ROSAT [20] and ASCA [21]. The PSPC instrument of the ROSAT Observatory has an angular resolution of 0′.5 and a spectral energy resolution $E/\Delta E \simeq 0.4$ at 1 keV. The SIS0 and SIS1 instruments (CCD arrays) of the ASCA Observatory have a spectral resolution $E/\Delta E \sim 50$ at energies 6 keV. The

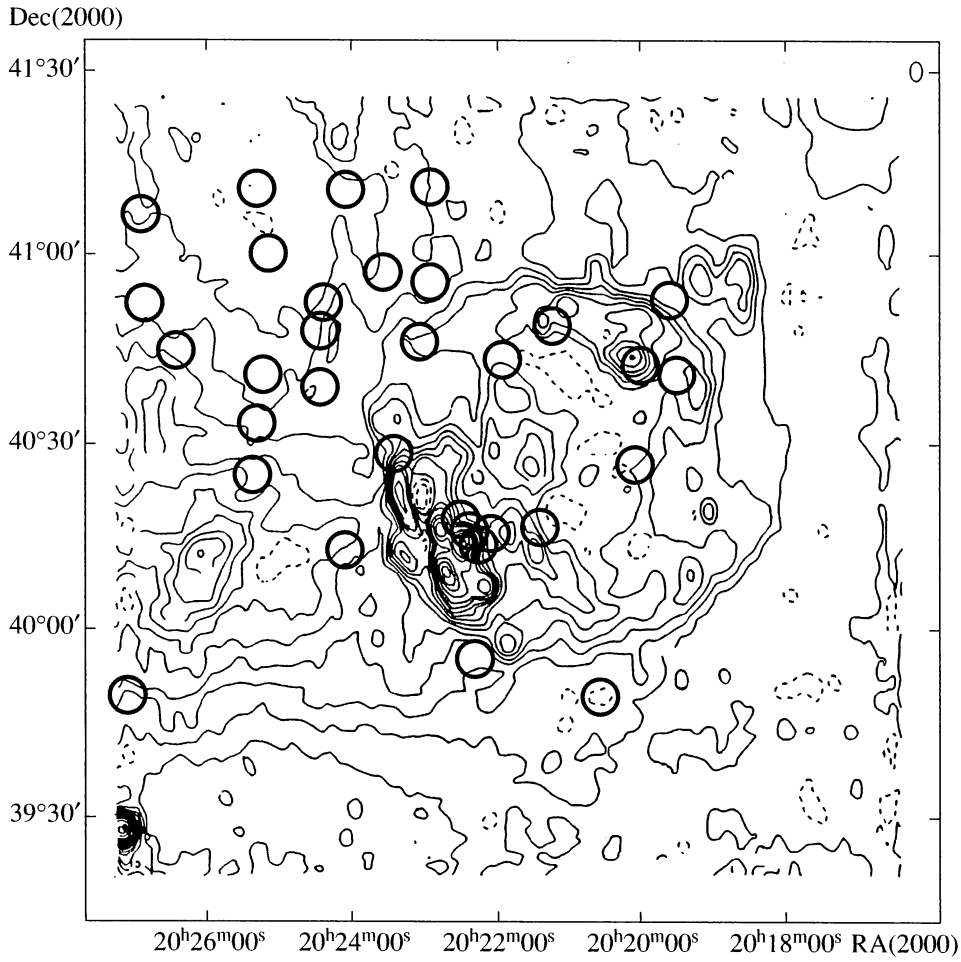

Fig. 1. Localization of interferometric rings of the Hα and [N II] 6584 Å lines superimposed on radio isophotes of G78.2+2.1 from [1].

point response function of the telescopes is characterized by a central peak with a FWHM of ~1′ and broad (~3′) wings. When all the four CCD arrays are used, the SIS field of view is 20′ × 20′. The SIS detectors are described in detail in [22].

We used the software package described in [23] to reduce the ROSAT data. Based on this packet, we chose exposure intervals with a minimum background, estimated the background level, and obtained exposure maps.

X-ray spectra were constructed from the ROSAT observations by using the XRAY package in the IRAF data-reduction system. Determination of the PSPC background in this package is based on [24]. We performed a spectral analysis in the recommended 0.2–2.0-keV energy band.

We used the 0.5–2.0-keV energy band, where the background effect is at a minimum, to analyze the images. The images were processed by wavelet transform analysis [25, 26].

The SNR G78.2+2.1 was observed in five PSPC/ROSAT pointings; the entire region corresponding to the bright radio source G78.2+2.1 was observed in the central part of the field of view, where the background effect is negligible. When weaker X-ray features far outside the radio SNR (the outer weak shell; see Subsect. 3.2) are analyzed, it should be borne in mind that these features can result in part from an enhancement of the PSPC background at the edge of the field of view. One of the pointings was centered on the SNR northern region, which simplified appreciably the background-subtraction procedure in this observation.

We analyzed the ASCA data by using the standard FTOOLS V4.1 software package for initial data reduction. This reduction involves choosing exposure intervals with a minimum background, estimating the background level, removing "hot pixels" of the SIS0 and SIS1 detectors, constructing the detector response matrix for the epoch of observation, and calibrating the instrumental energy scale.

The SIS/ASCA observations (three pointings) cover only the central part of G78.2+2.1 ($R \leq 15'$) and the region north of the SNR center ($0' \leq R \leq 30'$).

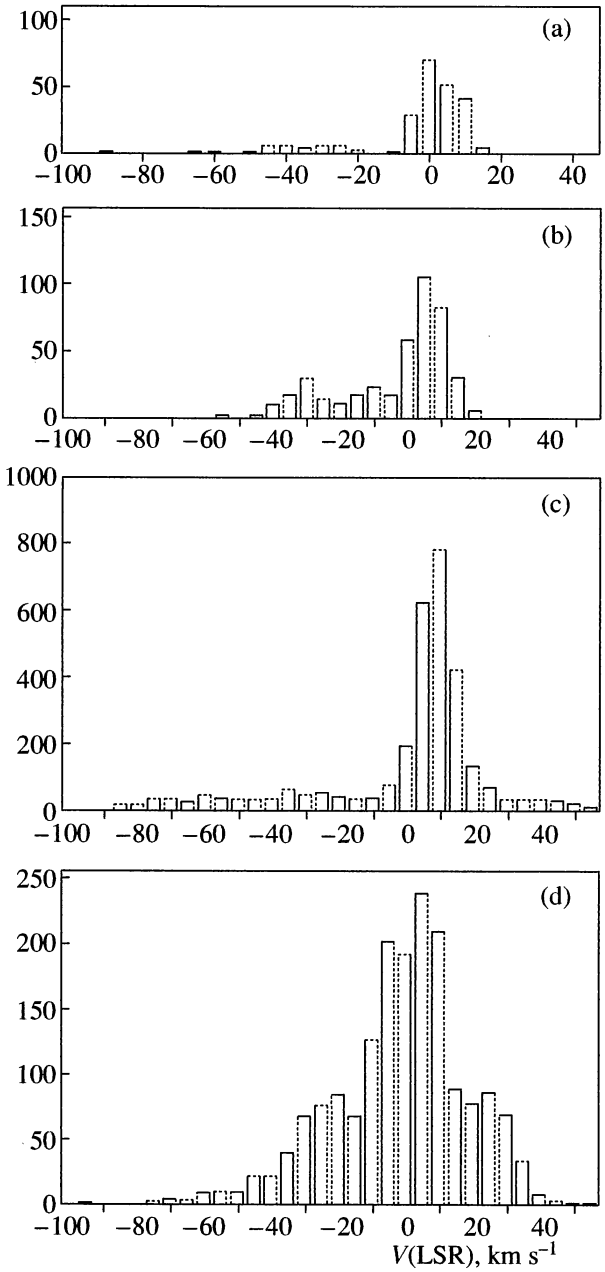

Fig. 2. Radial-velocity histograms for the Hα components: (a) in the SNR G78.2+2.1; (b) in the nearby region of the Cygnus complex X outside the bright SNR but inside the weak outer X-ray shell (see the text in Subsect. 3.2); (c) in the Cygnus X complex south and west of G78.2+2.1 at 2°–4° from the SNR center; (d) in the Cygnus X complex east and north of G78.2+2.1 (see text).

3.2. X-ray Image of the SNR

The X-ray (0.5–2.0 keV) brightness distribution of the SNR constructed by reducing the ROSAT data is shown in Fig. 3a. For comparison, Fig. 3b shows the distribution of synchrotron radio emission at a frequency of 1.4 GHz from [1] on the same scale. The X-ray image of the SNR G78.2+2.1 is characterized by a shell morphology; in general, there is agreement between the large-scale radio and X-ray structures of the SNR.

Figure 4 compares the fine X-ray emission features with the radio brightness distribution at 1.4 GHz as inferred from VLA aperture-synthesis observations. The radio isophotes were constructed from archival NRAO VLA Sky Survey (NVSS) data; the NVSS survey is described in detail in [27]. As follows from Fig. 4, there is a correlation between the features of the X-ray and radio images on scales of several arcminutes. This correlation is most noticeable at the eastern boundary, where the SNR most likely collides with a dense cloud of interstellar gas. In other regions, there is no one-to-one correspondence: Bright X-ray knots correspond to all compact bright radio features, but there are X-ray knots with no corresponding radio brightening.

The two elongated regions of reduced X-ray brightness, a wide band in the south (from RA = 20^h19^m, D = 39°40′ to RA = 20^h26^m, D = 39°40′) and a narrow band at the eastern boundary of G78.2+2.1 (RA = 20^h24^m, D = 40°0′–41°20′), are probably attributable to absorption; dust lanes are seen here on Palomar Atlas red maps.

The outer region of weak X-ray emission far outside the synchrotron source G78.2+2.1 and the bright X-ray SNR is clearly seen in Fig. 3a. This outer X-ray region is symmetric about G78.2+2.1; its geometrical center coincides with the SNR center, and the size is ~2°, which is twice the size of the bright shell.

The outer X-ray shell has been identified here for the first time. As was noted in Subsect. 3.1, weak features of the outer shell were observed at the edge of the field of view in four of the five telescope pointings and may partly result from an enhancement of the background toward the detector edge. One pointing was centered on the northern part of the SNR; the bright G78.2+2.1 shell, and the weak outer shell were observed at the center of the field of view. We therefore believe the reality of the northern part of the outer shell to be beyond question.

Figure 5 shows the SNR surface-brightness profiles. The SNR-averaged profile and the cuts in the northward and southward directions are presented. The profiles were constructed from three independent PSPC/ROSAT observations. The PSPC background effect does not change with radius in this figure, because we applied a correction for the instrument sensitivity. The difference in the background levels between the three observations can be easily determined from the flux in the central region $R \le 5'$, where the sky areas under study coincide. For comparison, the figure also shows the temperature profiles obtained in spectral analysis (see Subsect. 3.3).

Based on Figs. 3a and 5, we cannot unambiguously determine whether the detected outer weak emission is a shell or halo structure, because, as was pointed out

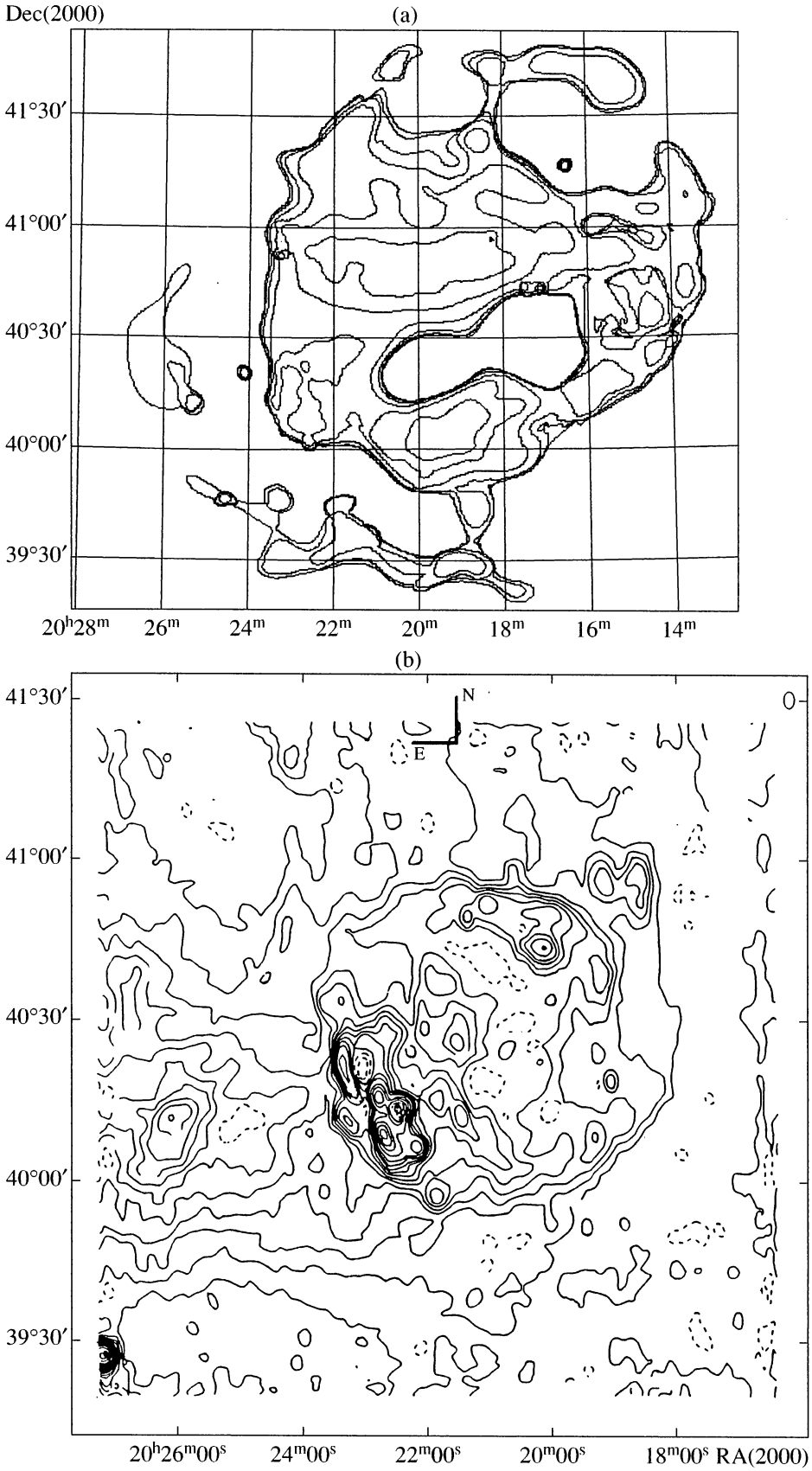

Fig. 3. (a) X-ray (0.5–2.0 keV) brightness distribution of the SNR as constructed from ROSAT data; (b) radio brightness distribution at 1.4 GHz from [1] on the same scale.

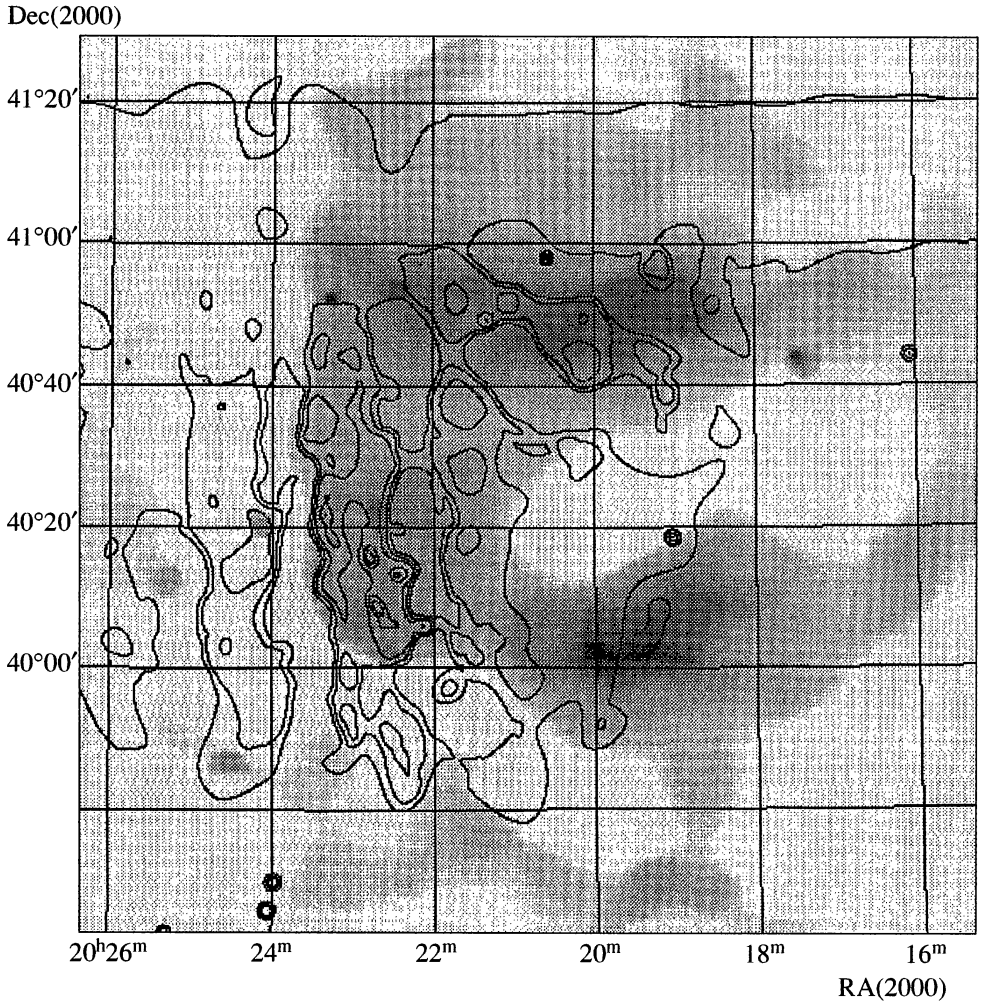

Fig. 4. X-ray (0.5–2.0 keV) brightness distribution as constructed from ROSAT data (black-and-white image) superimposed on the radio (1.4 GHz) isophotes constructed from archival NRAO VLA Sky Survey (NVSS) data.

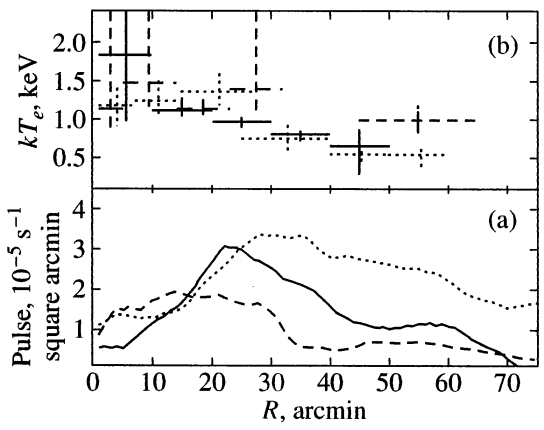

Fig. 5. (a) SNR surface-brightness profiles constructed from three independent PSPC/ROSAT observations: averaged over the remnant (solid line), in the northward (dotted line) and southward (dashed line) directions. (b) The temperature variation with distance from the SNR center; the lines designations are the same as those in (a). The data in the northward direction within 25′ were obtained from SIS/ASCA observations; the remaining values were obtained from PSPC/ROSAT observations.

above, the most pronounced dip in the eastern cut can be produced by the interstellar absorption, and the contribution of this cut to the average profile is significant.

3.3. X-ray Spectrum

Since an analysis of the ROSAT spectral data is complicated by low statistics and interstellar extinction, we first analyzed the ASCA data. We used the MEKAL model [28, 29] and the table of relative elemental abundances from [30] for the solar photosphere (Fe/H = 4.65×10^{-5} by the number of atoms).

Figure 6a shows the localization of the field of view for three ASCA pointings superimposed on the ROSAT image of the SNR. The average spectrum of this region is shown in Fig. 6b.

The spectral fit for this part of G78.2+2.1 in the ionization equilibrium plasma model corresponds to the temperature $kT_e = 1.4 \pm 0.1$ keV and the heavy-element abundance $Z = 0.27 \pm 0.1 Z_\odot$. Here, all confidence intervals correspond to a 68% confidence level. The derived

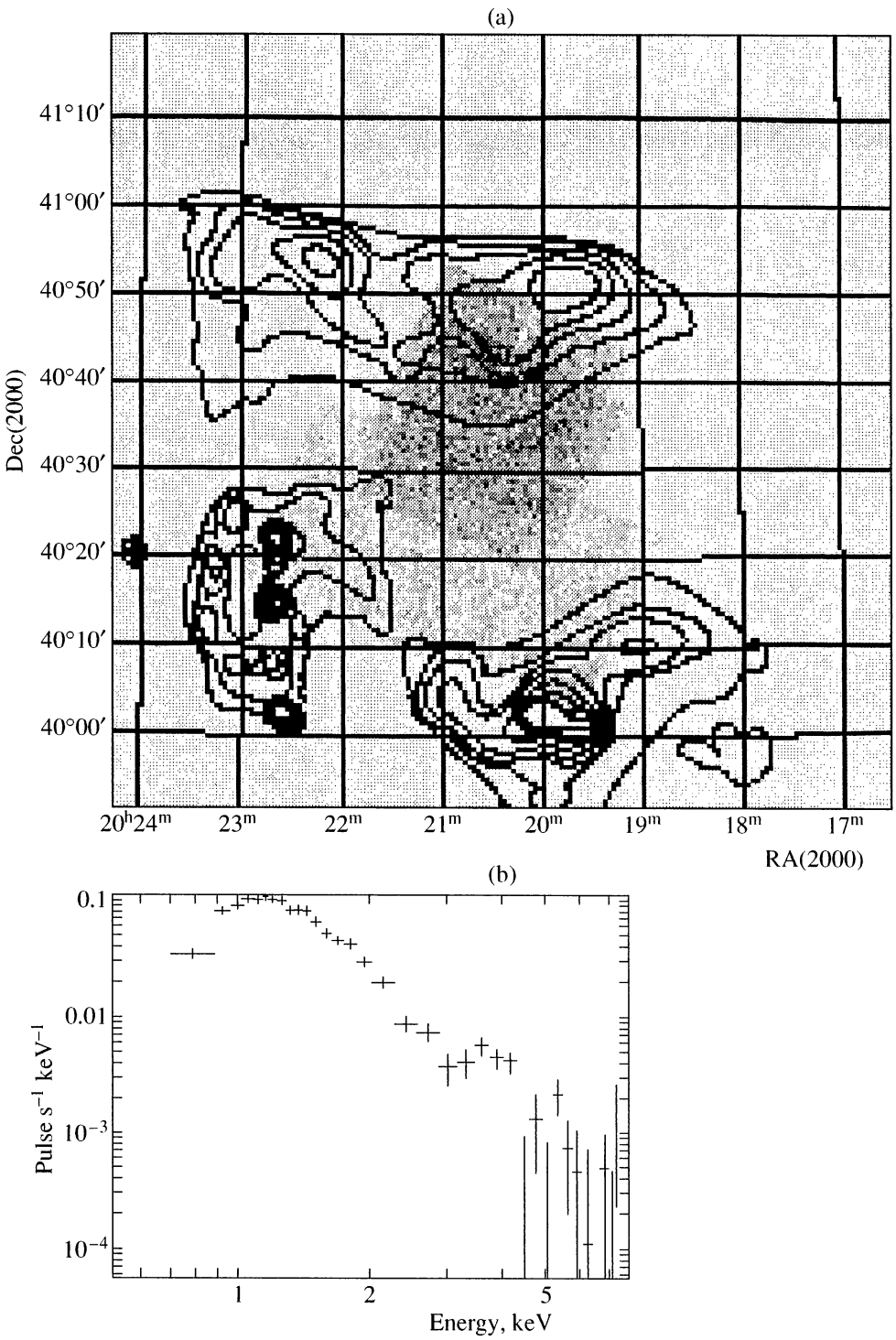

Fig. 6. (a) SIS/ASCA image of the central part of the SNR formed from the sum of four pointings superimposed on the surface brightness isolines as constructed from PSPC/ROSAT data. (b) The average SIS/ASCA spectrum of this region.

abundance agrees with the abundance for the Galactic thick disk [31]. Note that only the iron abundance affects the Z determination for solar elemental abundances.

The nonequilibrium ionization model [32], as applied to the ASCA data, yields a higher temperature (kT_e = 2.77 ± 0.4 keV), a comparable heavy-element abundance [Z = (0.24 ± 0.07)$Z_\odot$], and the ionization parameter $\log(n_0 t_i)$ = 11.06 s cm^{-3}; the confidence interval is (11.00–11.16). The parameter $n_0 t_i$, where n_0 is the ambient density of the interstellar medium and

t_i is the time after the shock passage, characterizes the advanced stage of ionization equilibrium (ionization age). The spectrum in Fig. 6b is "nonequilibrium" in that, in the presence of the iron-line emission peak at energy 1 keV characteristic of a 1.4-keV temperature, the continuum emission proves to be harder and corresponds to a temperature of 2.8 keV. Note also that, when the temperature in the PSPC/ROSAT and SIS/ASCA experiments is determined, the iron peak at 1 keV is of crucial importance. Under the assumption of ionization equilibrium, the derived temperatures are therefore the "ionization" ones.

When analyzing the ROSAT data, we took the elemental abundance that was deduced for the northern part of the SNR from ASCA measurements. The X-ray spectrum of the shell's extended bright features that fits the ROSAT data best assuming equilibrium plasma of this chemical composition yields $kT_e = 1.37 \pm 0.12$ and 1.00 ± 0.05 keV for the eastern and southern regions, respectively.

The profile of temperature variation with distance from the SNR center is shown in Fig. 5. The figure reveals a temperature constancy within 20′ at a 1.3-keV level and a subsequent drop in temperature, both in the northward and southward directions and, on average, over the SNR. The temperature at 60′ from the center is 0.5 keV, on average, over the SNR and in the north and twice as high in the east.

As we see from the figure, the outer X-ray shell (or the halo) is distinguished not only by its morphology but also differs from G78.2+2.1 in spectrum, although there is no sharp temperature drop.

The absorption of X-ray emission from the three bright SNR regions mentioned above corresponds to the column density $N(\mathrm{H}) = (1\text{–}3) \times 10^{21}$ cm^{-2}. The column density derived from the X-ray data is in close agreement with that deduced from direct 21-cm measurements: Landecker *et al.* [15] obtained $N(\mathrm{H\,I}) \approx 1.6 \times 10^{21}$ cm^{-2}, on average, over the SNR and a slightly higher value for its bright southeastern part.

Note that the Einstein observations with a lower angular resolution and lower sensitivity revealed emission from the brightest part of the SNR and yielded a similar temperature ($4 \times 10^6 \le T_X \le 5 \times 10^7$ K), density ($n_0 \approx 0.1\text{–}0.4$ cm^{-3}), and column density [$N(\mathrm{H\,I}) = 3 \times 10^{21} - 3 \times 10^{22}$ cm^{-2}] (see [17]).

The mean density and mass of X-ray emitting plasma

Region	Radius	n_X, cm^{-3}	M, $M_\odot$
Entire SNR	0′–40′	0.05 ± 0.01	47 ± 3
SNR + halo	0–60	0.04 ± 0.01	95 ± 10
Center	0–15	0.08 ± 0.01	4.0 ± 0.8
North	15–40	0.05 ± 0.01	11 ± 0.8
North	15–60	0.04 ± 0.01	27 ± 1.4
East	15–30	0.08 ± 0.01	5.9 ± 0.4
South	15–30	0.084 ± 0.004	8.3 ± 0.4
West	30–60	0.024 ± 0.003	14 ± 2

4. DISCUSSION

The distance $d \simeq 1.8$ kpc to G78.2+2.1 and its linear size of ~33 pc were determined from the dependence of surface radio brightness on SNR diameter [the so-called $\Sigma(D)$ dependence] by Higgs *et al.* [1] and Landecker *et al.* [15]. Using a more complete $\Sigma(D)$ dependence, which included a number of extragalactic calibration sources [3, 33], we obtained a similar SNR diameter of 29.4 pc and distance of 1.7 kpc from the flux density S (1 GHz) = 340 Jy [34]. At such a distance, the expected mean shell velocity in the Galactic rotation model by Dambis *et al.* [35] is ≈6–7 km s^{-1}; i.e., it agrees with the observed H II velocities in G78.2+2.1.

Since the error in the distance estimated from the $\Sigma(D)$ dependence can reach 30% and since the kinematic distances toward the Galactic longitudes $l = 70\text{–}80°$ are unreliable, we take $d = 1.7$ kpc as the most probable value. The masses and mean densities estimated for different parts of the SNR (the corresponding radii are indicated) by analyzing in detail the X-ray spectra with a radial-step width of 5′–10′ are given in the table. When calculating the "exact" mass, we determined the density, temperature, and absorption distributions in the plane of the sky. As we see from the table, the mass of the outer shell or the halo is approximately equal to the mass of the bright SNR G78.2+2.1.

For comparison, note that the masses estimated from the total SNR luminosity by assuming spherical and shell ($\Delta R/R \simeq 0.3$) models are 140 and $110 M_\odot$, respectively. For such a mass estimate, we took the coefficient of volume luminosity in accordance with the temperature $kT = 1.4$ keV and metallicity $Z = 0.27 Z_\odot$ derived above; the MEKAL model was used. The SNR shell model is seen to yield the estimate that is closest to the exact value in the table: $95 \pm 10 M_\odot$.

The temperatures $T_X = 1.6 \times 10^7$ K (for ionization equilibrium plasma) and $T_X = 3.2 \times 10^7$ K (in the absence of ionization equilibrium) deduced from the X-ray spectrum of the bright shell are typical of the gas behind an adiabatic shock front. The corresponding shock velocity is $V_s = (1\text{–}1.5) \times 10^3$ km s^{-1}.

The mass of the postshock gas in a SNR is the principal parameter that characterizes its evolutionary status [3]; the X-ray plasma mass $M \approx 50\text{–}100 M_\odot$ suggests a transition from the phase of free expansion to the phase of adiabatic expansion (Sedov phase). Our mass estimate for the hot plasma in the entire G78.2+2.1 shell agrees with the mass determined from IRAS observations; Saken *et al.* [36] identified a spherical infrared shell with the SNR and estimated the total mass of its gas to be $M = 100 M_\odot$.

Assuming the radius $R = 15$ pc and the post-shock temperature $T_s = (1.6\text{–}3.2) \times 10^7$ K for the standard explosion kinetic energy $E = 10^{51}$ erg, we obtain an age

of (4–6) × 10^3 years and the ambient gas density $n_0 = 0.14$–0.3 cm^{-3} for the SNR at the adiabatic phase in a homogeneous medium. This density is in agreement with the initial density ($n_0 = 0.32$ cm^{-3}) independently estimated from the mass of the infrared shell by assuming that the gas swept up from the inner volume concentrates in it.

Thus, the X-ray observations of the bright source G78.2+2.1 lead to a self-consistent model for a young SNR at an early stage of adiabatic expansion in a medium of relatively low density.

At this stage, the optical emission from the SNR must be weak: Intense radiative cooling in a homogeneous medium of density $n_0 = 0.3$ cm^{-3} begins considerably later, when the SNR radius, expansion velocity, and age are, respectively, $R_c \approx 30$ pc, $v_c \approx 250$ km s^{-1}, and $t_c \approx 5 \times 10^4$ years.

Indeed, as yet no bright optical shell that could be unambiguously correlated with G78.2+2.1 (or with the outer X-ray shell) has been detected. The optical emission from the SNR may be represented by weak filaments in the west with the $I(\mathrm{H}\alpha)/I([\mathrm{S\ II}])$ ratio typical of SNRs [37]. However, filaments emitting in [S II] 6717/6731 Å are clearly seen on photographs from the atlas of Parker *et al.* [38] far outside G78.2+2.1 and the weak outer shell. To reach a more definitive conclusion, we need the relative line intensities in the spectra of these filaments inside and outside the SNR. As we made sure in Subsect. 2.2, the Hα emission toward G78.2+2.1, including the filaments mentioned above, does not differ significantly in radial velocities from the emission of the nearby part of Cygnus X.

We therefore cannot rule out the possibility that the optical nebulae toward G78.2+2.1 are H II regions. This is consistent with the radio spectrum of G78.2+2.1, which exhibits variations in the spectral index attributable to the superposition of two components: Synchrotron radiation of the SNR and thermal radiation of the H II regions [4]. The contribution of thermal radio emission is largest in the region of DR4 and the bright nebula near γ Cygni [1, 11]. Here, the expanding G78.2+2.1 shell most likely collides with a dense cloud, as suggested by the sharp brightness gradient and the nonspherical plane boundary of the bright X-ray and radio shells (Fig. 4). This is also evidenced by the two small CO knots detected by Fukui and Tatematsu [39] at $V(\mathrm{LSR}) = -(3$–$1)$ and $+(1$–$3)$ km s^{-1}, which closely coincide with the regions of local brightening of the radio shell and anticorrelate with the X-ray brightness.

H I observations revealed a geometrically thick, slowly expanding shell around the SNR [14, 15] and high-velocity cloudlets [15, 16]. The mean velocity of the H I shell is $V(\mathrm{LSR}) = +3$ km s^{-1}, the probable expansion velocity is ~10 km s^{-1}, the mass is $8 \times 10^3 M_\odot$, the mean density is ≈2.5 cm^{-3}, and the kinetic energy does not exceed a few percent of the energy of a standard supernova explosion (10^{51} erg) [14]. As was pointed out by Gosachinskii *et al.* [14], judging by the energetics, the outer H I shell could be produced both by the supernova explosion and by the stellar wind from the supernova progenitor. Since the X-ray emission from G78.2+2.1 suggests an early adiabatic phase, the latter currently seems more justified.

The existence of an outer weak X-ray shell far outside the synchrotron radio source G78.2+2.1 and the bright X-ray SNR undoubtedly requires an observational confirmation. If the reality of the weak X-ray shell (or the halo) is confirmed, then the question of its nature and relationship to the H I shell will arise.

The coexistence of a cold H I shell and a weak outer X-ray shell of virtually the same size could be explained in principle by the fact that the supernova explosion occurred at the boundary of an extended dense cloud with a sharp density gradient. In this case, the SNR has the peculiar shape of two connected hemispheres of different sizes at different evolutionary stages because of the difference in initial ambient density. The part of the SNR in the dense gas may be represented by the bright X-ray source G78.2+2.1 and the extended H I shell produced by the progenitor's stellar wind in the cloud, while the part of the SNR in the low-density intercloud medium may be represented by the outer X-ray shell. The SNR VRO42.05.01 [40] is an example of such a structure for the direction of density gradient perpendicular to the line of sight, which is "favorable" for the observer.

If the line of sight is directed along the density gradient, we will see the X-ray and H I shells coinciding "by chance" in projection onto the plane of the sky. However, the fact that the outer X-ray shell has a lower temperature than the bright G78.2+2.1 shell is in poor agreement with this model.

An explanation of the coexistence of the H I shell and the two X-ray shells in the model of a supernova explosion in the cavity swept up by the supernova progenitor wind is of greater interest. The evolution of a SNR in a cavity has long been analyzed by many authors (see [41] and references therein). The key point here is the collision of the SNR with the dense cavity walls (before the collision, the supernova shell expands virtually without deceleration; after the collision, the radiative phase of the postshock gas sets in very rapidly). Depending on the mass ratio of the supernova shell and the shell swept up by the wind, as well as on the velocity at which the shock triggered by the supernova impinges on the cavity walls, one might expect the formation of a double X-ray shell at least in two stages. X-ray emission from the gas heated by the blast wave in the swept-up shell and from the gas behind the reflected shock in the SN ejecta can be observed at the early stage, until the mass of the postshock gas in the swept-up shell does not exceed the ejected mass by more than a factor of 40–50. In this case, the inner shell must be hotter and, under certain conditions, can be brighter than the outer one.

Subsequently, the H I shell swept up by the wind is fragmented because of the Rayleigh–Taylor instability at the contact surface between the gas behind the direct shock front and that behind the reflected shock front. As a result, an outer X-ray shell representing the gas behind the direct shock front, which has mainly passed the H I shell through breaks between its individual fragments, can be formed. The neutral hydrogen associated with the SNR G78.2+2.1 actually exhibits a distinct clumpy structure, as suggested by the small-scale ($\approx$6–10′) high-velocity H I cloudlets detected by Braun and Strom [16] and Landecker *et al.* [15].

Observations of the SNR W44 provide evidence that the H I shell swept up by the wind may turn out to be inside the SNR. Koo and Heiles [42] explained an expanding H I shell (of radius 9 pc) inside a synchrotron radio shell (of radius 15 pc) in terms of this model. The age of the pulsar associated with W44 is $\approx 3 \times 10^4$ years; W44 exhibits a more "advanced" stage of interaction with the swept-up shell than does G78.2+2.1. Here, there are all the signatures of the radiative phase: bright optical filaments and X-ray emission with a relatively low temperature of $T_e = (4–8) \times 10^6$ K enhanced toward the center.

5. CONCLUSION

Our optical and X-ray observations of G78.2+2.1 and their comparison with radio-continuum studies and IRAS data provide evidence for a young adiabatic SNR ($M_{X-ray} = 95 \pm 10 M_\odot$, $V_s \approx 10^3$ km s^{-1}, $t \approx (5–6) \times 10^3$ years).

In general, there is agreement between the large-scale X-ray and radio structures of G78.2+2.1; the X-ray image exhibits a shell structure ($\Delta R/R \approx 0.3$). A comparison with the radio map at $\nu = 1.4$ GHz constructed from archival VLA data reveals the coincidence of features at the eastern SNR boundary on scales of several arcminutes.

A weak X-ray emission (an outer shell or halo) has been detected far outside the synchrotron radio source G78.2+2.1 for the first time. The outer shell size of $\approx 2°$ is twice the size of the bright source G78.2+2.1.

We conclude that the previously identified [14, 15], slowly expanding massive H I shell around G78.2+2.1 was produced by the stellar wind from the supernova progenitor. The SNR expansion mainly took place inside the cavity swept up by the wind; the interaction with the dense walls of the swept-up shell has begun relatively recently. The formation of the weak outer X-ray shell we detected can be explained in terms of the theory of SNR evolution in the cavity swept up by the progenitor's stellar wind [41].

We emphasize that both alternatives considered in Sect. 4 to account for the outer X-ray shell and its coexistence with the H I shell are speculative so far. To elucidate the nature of the outer shell or the halo and to determine the evolutionary status of the SNR requires the following:

First, a confirmation of the existence of outer weak X-ray emission and determination of its structure: a shell or a plateau.

Second, a confirmation of the existence of an H I shell. Recall that Landecker *et al.* [15] detected an expanding H I ring around G78.2+2.1 only by observing two clouds with markedly differing radial velocities, one in emission and the other in absorption. The H I ring structure identified by Gosachinskii *et al.* [14], into which the SNR fits well in the plane of the sky, is also ambiguous. The authors pointed out that the distribution of 21-cm emission in the vicinity of G78.2+2.1 is extremely nonuniform; the western part of this shell is identified unreliably, because it is projected onto the large shell around the entire Cygnus X complex; the pattern is distorted by the emission from the bright source Cygnus A in the beam wing.

Third, special observations aimed at searching for optical emission from the SNR are required. The lower temperature of the outer X-ray shell suggests that the radiative cooling in this region may be already significant, and the optical emission can be noticeable at least in the outer region outside G78.2+2.1, if not in the SNR itself.

Fourth, and this is the key point, searches for the corresponding outer radio-continuum structure are required. Only after the radio spectrum associated with the outer X-ray shell has been determined can we elucidate its nature and, accordingly, the evolutionary status of the SNR.

ACKNOWLEDGMENTS

We used the observational data retrieved from the HEASARC archive. This study was supported by the Russian Foundation for Basic Research (project no. 98-02-16032) and the Astronomy Program (project no. 1.3.1.2).

REFERENCES

1. L. A. Higgs, T. L. Landecker, and R. S. Roger, Astron. J. **82**, 718 (1977).
2. H. L. Wendker, L. A. Higgs, and T. L. Landecker, Astron. Astrophys. **241**, 551 (1991).
3. T. A. Lozinskaya, *Supernovae and Stellar Wind in the Interstellar Medium* (AIP, New York, 1992).
4. X. Zhang, Y. Zheng, T. L. Landecker, *et al.*, Astron. Astrophys. **324**, 641 (1997).
5. S. Van den Bergh, A. P. Marcher, and Y. Terzian, Astrophys. J., Suppl. Ser. **26**, 19 (1973).
6. T. A. Lozinskaya, Astron. Zh. **52**, 515 (1975).
7. H. M. Johnson, Astrophys. J. **206**, 243 (1976).
8. V. P. Arkhipova, N. A. Gorynya, V. F. Esipov, *et al.*, Astron. Tsirk., No. 810, 4 (1974).

9. V. P. Arkhipova and T. A. Lozinskaya, Astron. Zh. **55**, 1320 (1978).
10. T. A. Lozinskaya, Pis'ma Astron. Zh. **3**, 306 (1977) [Sov. Astron. Lett. **3**, 163 (1977)].
11. J. Baars, H. R. Dickel, and H. J. Wendker, Astron. Astrophys. **62**, 13 (1978).
12. A. J. Landecker, Astron. J. **89**, 95 (1984).
13. A. Piepenbrink and H. J. Wendker, Astron. Astrophys. **191**, 313 (1988).
14. I. G. Gosachinskii, T. A. Lozinskaya, and V. V. Pravdikova, Astron. Zh., 1999 (in press).
15. T. L. Landecker, R. S. Roger, and L. A. Higgs, Astron. Astrophys., Suppl. Ser. **39**, 133 (1980).
16. R. Braun and R. G. Strom, Astron. Astrophys., Suppl. Ser. **63**, 345 (1986).
17. L. A. Higgs, T. L. Landecker, and F. D. Seward, *Supernova Remnants and Their X-ray Emission, IAU Symp. 101*, Ed. by J. Danziger and P. Gorenstein (Reidel Publ., Dordrecht, 1983), p. 281.
18. J. A. Esposito, S. D. Hunter, G. Kanbach, *et al.*, Astrophys. J. **461**, 820 (1996).
19. K. T. S. Brazier, G. Kanbach, A. Carraminana, *et al.*, Mon. Not. R. Astron. Soc. **281**, 1033 (1996).
20. J. Truemper, Adv. Space Res. **2**, 241 (1983).
21. Y. Tanaka, H. Inoue, and S. S. Holt, Publ. Astron. Soc. Jpn. **46**, L37 (1994).
22. B. E. Burke, R. W. Mountain, D. C. Harrison, *et al.*, IEEE Trans., **EED**-38, 1069 (1991).
23. S. L. Snowden, D. McCammon, D. N. Burrows, *et al.*, Astrophys. J. **424**, 714 (1994).
24. P. P. Plucinsky, S. L. Snowden, U. G. Briel, *et al.*, Astrophys. J. **418**, 519 (1993).
25. A. A. Vikhlinin, Candidate's Dissertation, IKI RAN (Space Research Inst., Russian Academy of Sciences) (Moscow, 1995).
26. S. A. Grebenev, W. Forman, C. Jones, *et al.*, Astrophys. J. **445**, 607 (1995).
27. J. J. Condon, W. D. Cotton, E. W. Greisen, *et al.*, Astron. J. **115**, 1693 (1998).
28. R. Mewe, E. H. B. M. Gronenschild, and G. H. J. Oord, Astron. Astrophys., Suppl. Ser. **62**, 197 (1985).
29. R. Mewe and J. Kaastra, *Internal SRON-Leiden Report* (1995).
30. E. Anders and N. Grevesse, Geochim. Cosmochim. Acta **53**, 197 (1989).
31. L. S. Lyubimkov, *Stellar Chemical Composition: Methods and Results of Analysis* [in Russian], Ed. by A. A. Boyarchuk (IPR Astroprint, Odessa, 1995).
32. J. P. Hughes and D. J. Helfand, Astrophys. J. **291**, 544 (1985).
33. T. A. Lozinskaya, Pis'ma Astron. Zh. **7**, 29 (1981) [Sov. Astron. Lett. **7**, 17 (1981)].
34. D. A. Green, *A Catalogue of Galactic SNRs (1996 August Version)* (Mullard Radio Astron. Obs., Cambridge, 1996).
35. A. K. Dambis, A. M. Mel'nik, and A. S. Rastorguev, Pis'ma Astron. Zh. **21**, 331 (1995) [Astron. Lett. **21**, 291 (1995)].
36. J. M. Saken, R. A. Fesen, and J. M. Shull, Astrophys. J., Suppl. Ser. **81**, 715 (1992).
37. S. Van den Bergh, Astrophys. J., Suppl. Ser. **38**, 119 (1978).
38. R. A. Parker, Th. R. Gull, and R. P. Kirshner, *An Emission-Line Survey of the Milky Way* (NASA, Washington DC, 1979).
39. Y. Fukui and K. Tatematsu, *Supernova Remnants and the Interstellar Medium, IAU Coll. 101*, Ed. by R. S. Roger and T. L. Landecker (Cambridge University, Cambridge, 1988), p. 261.
40. T. L. Landecker, S. Pineault, D. Routledge, *et al.*, Astrophys. J. Lett. **261**, L41 (1982).
41. G. Tenorio-Tagle, M. Rozyczhka, J. Franco, *et al.*, Mon. Not. R. Astron. Soc. **251**, 318 (1991).
42. B.-C. Koo and C. Heiles, Astrophys. J. **442**, 679 (1995).

Translated by V. Astakhov